Inorganic Chemistry

Article

pubs.acs.org/IC

Two Isotypic Transition Metal Germanophosphates $M^{II}_4(H_2O)_4[Ge(OH)_2(HPO_4)_2(PO_4)_2]$ (M^{II} = Fe, Co): Synthesis, Structure, Mössbauer Spectroscopy, and Magnetic Properties

Ya-Xi Huang,*[,†] Xin Zhang,[†] Xuan Huang,[†] Walter Schnelle,[§] Jun Lin,[∥] Jin-Xiao Mi,[†] Mei-Bo Tang,[‡] and Jing-Tai Zhao[‡]

[†]Department of Materials Science and Engineering, College of Materials, Xiamen University, Xiamen 361005, China

[‡]State Key Laboratory of High Performance Ceramics and Superfine Microstructure, Shanghai Institute of Ceramics, Chinese Academy of Sciences, Shanghai 200050, China

[§]Max-Planck-Institut für Chemische Physik fester Stoffe, Nöthnitzer Straße 40, Dresden 01187, Germany

[∥]Key Laboratory of Nuclear Analysis Techniques, Shanghai Institute of Applied Physics, Chinese Academy of Sciences, Shanghai 201800, China

Supporting Information

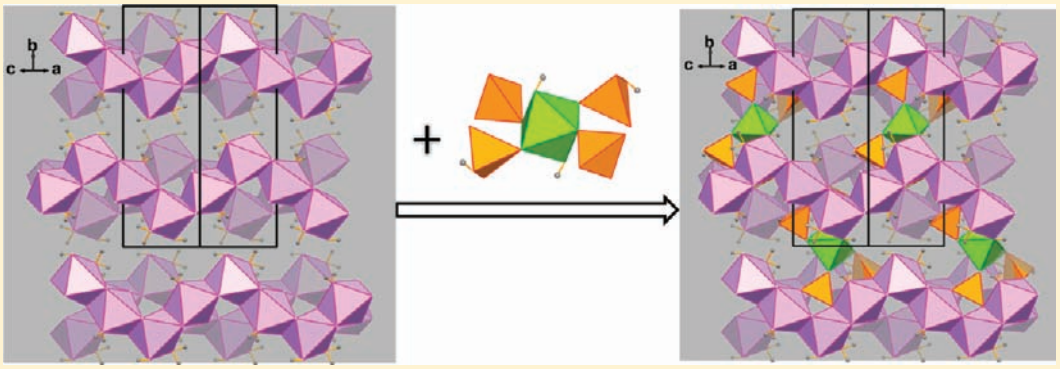

ABSTRACT: Synthetic, structural, thermogravimetric, Mössbauer spectroscopic, and magnetic studies were performed on two new isotypic germanophosphates, $M^{II}_4(H_2O)_4[Ge(OH)_2(HPO_4)_2(PO_4)_2]$ (M^{II} = Fe, Co), which have been prepared under hydro-/solvo-thermal conditions. Their crystal structures, determined from single crystal data, are built from zigzag chains of $M^{II}O_6$-octahedra sharing either trans or skew edges interconnected by $[GeP_4O_{14}(OH)_4]^{8-}$ germanophosphate pentamers to form three-dimensional neutral framework structure. The edge-sharing $M^{II}O_6$-octahedral chains lead to interesting magnetic properties. These two germanophosphates exhibit a paramagnetic to antiferromagnetic transition at low temperatures. Additionally, two antiferromagnetic ordering transitions at around 8 and 6 K were observed for cobalt compound while only one at 19 K for the iron compound. Low-dimensional magnetic correlations within the octahedral chains are also observed. The divalent state of Fe in the iron compound determined from the Mössbauer study and the isothermal magnetization as well as thermal analyses are discussed.

1. INTRODUCTION

Microporous materials based on transition metal elements have been extensively studied due to their potential catalytic, electrical, optical, and magnetic properties.[1,2] Some interesting properties which transition metal phosphates have demonstrated are inaccessible to zeolites and other frameworks based on main-group elements only. For instance, lithium iron phosphate ($LiFePO_4$), with an olivine structure, is a potential cathode material for lithium batteries.[3,4] Vanadyl pyrophosphate $(VO)_2P_2O_7$ has been claimed to be an active phase of commercial catalysts which are capable to directly transform *n*-butane to maleic anhydride.[5] On the other hand, main group elements, e.g., Si, Al, and P, provide quite diverse structural chemistry. Recently, building units for microporous materials have been extended to germanate. Various germanates with zeotype structures have been successfully synthesized, in which GeO_4 tetrahedra, GeO_6 octahedra, and sometimes even GeO_5 trigonal bipyramids are joined through shared corners/edges to form frameworks.[6−12] As a branch of germanate, germanophosphates, however, have not been fully exploited. Only a few $M^IGe_2(PO_4)_3$ (M^I = Li, Na, K, Ag, Cu(I))[13−16] materials with NASICON type compositions have been prepared by conventional solid-state reactions with synthetic temperatures above 1000 °C. Germanophosphates based on transition metal are even rarer. Up to now, only four compounds are known.

Received: December 28, 2011
Published: February 15, 2012

   dx.doi.org/10.1021/ic202773p | *Inorg. Chem.* 2012, 51, 3316−3323

$Cd_5(PO_4)GeO_4$[17] was obtained by solid-state synthesis at high temperature and with a dense structure of CdO_7 polyhedra, CdO_6 octahedra, PO_4 tetrahedra, and GeO_4 tetrahedra by sharing the O-corners. Zinco-germanophosphate, (DABCO)·$ZnGe(HPO_4)_3$,[18] is characterized by a tetrahedral framework structure built from ZnO_4, GeO_4, and PO_4 tetrahedra. $[Cu(H_2O)_2(OH)]_2Ge(PO_4)_2$[19] and $CdGe(OH)_3PO_4$[20] feature two types of open frameworks without any templates (such as alkali metals and amines) synthesized under mild conditions. $[Cu(H_2O)_2(OH)]_2Ge(PO_4)_2$[19] consists of Cu−O−Cu chains of CuO_6 octahedra by corner-sharing interconnected by loop branched octahedral-tetrahedral germanophosphate chains of alternating germanate and phosphate units. $CdGe(OH)_3PO_4$[20] is built from edge-sharing CdO_6 octahedral chains interconnected by corner-sharing GeO_6 chains and PO_4 tetrahedra. Note that these transition metal based compounds did not show such interesting magnetic properties as phosphates. Thus, in an attempt to obtain microporous compounds with interesting magnetic properties, our studies focus on compounds composing both transition metal and germanophosphate. As a result, we obtained the first iron germanophosphate and cobalt germanophosphate with the same structure-type. These two isotypic transition metal germanophosphates $M^{II}_4(H_2O)_4[Ge(OH)_2(HPO_4)_2(PO_4)_2]$ (M^{II} = Fe, Co) (denoted as **FeGePO** and **CoGePO**, respectively) have been synthesized by hydro-/solvothermal methods and exhibit a three-dimensional (3-D) structure containing zigzag M^{II}-octahedral single chains by edge-sharing, which have interesting magnetic properties.

2. EXPERIMENTAL SECTION

2.1. Synthesis. The isotypic compounds have been synthesized under mixed hydro-/solvo-thermal conditions with 1,2-propanediol and water as solvents in the presence of the structure-directing agent triethylamine (TEA). For **CoGePO**, in a typical synthesis route GeO_2 (0.070 g, 0.7 mmol) and $CoCl_2·6H_2O$ (0.237 g, 1 mmol) were dissolved in H_2O (2 mL, 111 mmol). Then TEA (2 mL, AR, 14.4 mmol) and H_3PO_4 (85%, 1 mL, 14.6 mmol) were added to the above solution dropwise. Finally, 1,2-propanediol (2 mL, 21 mmol) was added under constant stirring. The mixture (molar ratio of GeO_2/$CoCl_2·6H_2O$/H_3PO_4 = 0.7:1:14.6) with an initial pH of 4 was transferred into a Teflon-lined stainless-steel autoclave (15 mL in volume) and heated at 150 °C for 4 days under static conditions. The resulting product was filtered, washed with deionized water, and dried in air to result in purple pseudo octahedral crystals in high yield (above 85%, based on Co). The X-ray powder diffraction pattern of **CoGePO** indicated that the product was a new phase. It is consistent with the structure determined by single crystal diffraction data (see Figure S2 in the Supporting Information).

For the synthesis of **FeGePO**, when applying a similar experimental method but using $FeCl_2·4H_2O$ (0.198 g, 1 mmol) instead of $CoCl_2·6H_2O$, no single phase was obtained but a mixture of Large-sized light green single crystals of **FeGePO**, suitable for single crystal XRD analysis, and a minor needle phase of $Fe(H_2PO_4)_2·2H_2O$.[21] In order to get the pure phase for further investigation on physical properties, various synthesis conditions were explored. It turned out that the replacement of $FeCl_2·4H_2O$ by iron powder leads to the pure phase. Thus $FeCl_2·4H_2O$ was used to synthesize single crystals for structure determination while Fe powder was applied to produce a pure phase of **FeGePO**.

Further investigations on both compounds showed that both compounds could be obtained in the composition range of (0.7−1) GeO_2:(1) $CoCl_2.6H_2O$/Fe:(10.8−14.4) TEA:(111) H_2O:(10.95−18.25) H_3PO_4:(21) 1,2-propanediol. The amount of H_3PO_4 is critical; an excessive amount of H_3PO_4 (V > 1.5 mL) resulted in pure $Ge(OH)PO_4$.[22] The reaction temperature, reaction time, and type of amine can be tuned in a wide range. The temperature can be in the range of 120−190 °C, the treating time can range from 3 to 14 days, and TEA can be replaced by pyridine. Although TEA/pyridine was not involved in the coordination of the title compound, it played an important role in the formation of the title compounds. Without TEA/pyridine, the title compounds could not be obtained, even though other conditions were kept unchanged.

2.2. Methods. In order to determine the chemical composition of the title compounds, elemental analyses were carried out by means of inductively coupled plasma-optical emission spectroscopy (ICP-OES) on a Varian Vista RL spectrometer with radial plasma observation. IR spectra were recorded on a Spectrum 100 Optical (PerkinElmer) equipped with attenuated total reflectance. The phase purity has been checked by means of powder X-ray diffraction. The diffraction patterns were recorded on an X-ray powder diffractometer of Huber Image Foil Guinier Camera G670 (Cr $K_{\alpha 1}$-radiation, germanium (111) monochromator). The sizes and morphologies of the synthesized compounds were observed using a field emission scanning electron microscope (FE-SEM, LEO-1530). Thermogravimetric analyses (TGA) were investigated on STDQ600 (TA Instruments) with heating rates of 10 K min^{-1} from room temperature to 800 °C in a gas flow of 20 mL min^{-1}. In order to determine the oxidation state of Co and Fe in these compositions, magnetic measurements were carried out on a SQUID magnetometer (Quantum Design, MPMS XL-7). The oxidation state of Fe was further studied by Mössbauer spectroscopy. The ^{57}Fe transmission Mössbauer spectra for powder samples were measured at room temperature using a ^{57}Co/Rh source.

2.3. Crystal Structure Determination. Suitable single crystals of **FeGePO** and **CoGePO** (Figure 1) have been selected and checked first under polarized microscope for single-crystal X-ray diffraction. The data were collected at 173 K on a Rigaku R-AXIS RAPID image plate diffractometer with graphite monochromated Mo Kα radiation (λ = 0.710 73 Å; 50 KV/40 mA; scan types, ϕ and ω) with a maximum of 2θ = 54.9°. The crystal structures were solved in the space group $P2_1/n$ by direct methods and refined by full-matrix least-squares methods using the SHELX programs[23] included in the WinGX package.[24] After anisotropic displacement parameters had been included in the refinement, the hydrogen atoms of the water molecules (O1 and O2) and hydroxyl group (O9) were located from difference Fourier maps, and their atomic coordinates were included in the refinement subject to restraint of the O−H bond lengths to 0.82 Å. While the hydrogen atom bonded to O8 were generated geometrically without further refinement. Relevant crystallographic details are given in Table 1, and selected bond lengths and angles as well as bond valence sums are given in Table 2. Further crystallographic information (excluding structure factors) can be obtained free of charge from Fachinformationszentrum Karlsruhe, 76344, Eggenstein-Leopoldshafen, Germany (e-mail, crysdata@fiz-karlsruhe.de), on quoting the depository number CSD-424195 and CSD-424196 for **FeGePO** and **CoGePO**, respectively.

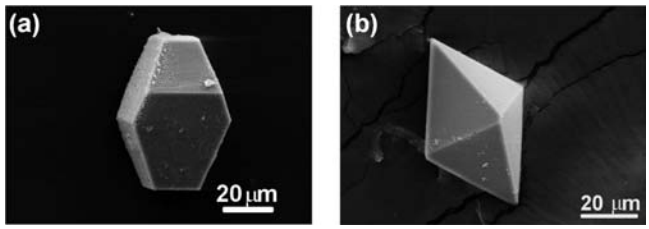

Figure 1. SEM images of single crystals: (a) **FeGePO** and (b) **CoGePO**.

3. RESULTS AND DISCUSSION

3.1. Crystal Structure Description. The crystal structures of the isotypic title compounds are built from one-dimensional zigzag octahedral chains interconnected by $[GeP_4O_{14}(OH)_4]^{8-}$

dx.doi.org/10.1021/ic202773p | Inorg. Chem. 2012, 51, 3316−3323

Table 1. Crystallographic Data and Refinement Results of $M^{II}_4(H_2O)_4[Ge(OH)_2(HPO_4)_2(PO_4)_2]$ (M^{II} = Fe, Co) (Denoted as FeGePO and CoGePO)

compound	FeGePO	CoGePO
space group	monoclinic, $P2_1/n$ (no. 14)	
a (Å)	6.4809(3)	6.4328(5)
b (Å)	16.3551(8)	16.267(2)
c (Å)	7.6041(2)	7.5154(6)
β (deg)	98.525(1)	97.804(3)
V (Å^3)/Z	797.10(6) /2	779.16(11)/2
ρ_{calcd} (g cm^{-3})	3.266	3.394
μ (mm^{-1})	5.947	6.618
crystal size (mm^3)	0.13 × 0.13 × 0.10	0.10 × 0.05 × 0.05
radiation/temp	Mo Kα/173 K	
R_{int}/R_σ	0.0349/0.0274	0.0427/0.0347
no. all/$I > 2\sigma(I)$	1814/1701	1778/1591
no. of parameters	157	158
R1 ($I > 2\sigma(I)$)	0.0234	0.0306
wR2 (all data)	0.0589	0.0752
GOF (for F^2)	1.048	1.209
residual electron density (max/min) (e Å^{-3})	−0.734/0.720	−0.719/0.773

Table 2. Crystal Structures of FeGePO and CoGePO: Selected Bond Lengths (Å) and Angles (deg), Together with the Bond Valence Sums (BVS)

FeGePO		CoGePO		
bond	distance (Å)	bond	distance (Å)	BVS
Ge1−O8$_H$ × 2	1.8592(19)	Ge1−O8$_H$ × 2	1.857(3)	**FeGePO**
−O11 × 2	1.8768(18)	−O11 × 2	1.865(3)	Ge1: 4.204
−O10 × 2	1.9042(19)	−O10 × 2	1.896(3)	Fe1: 2.049
Fe1−O6	2.1157(19)	Co1−O6	2.099(3)	Fe2: 1.974
−O7	2.1261(19)	−O7	2.083(3)	P1: 4.758
−O8$_H$	2.129(2)	−O8$_H$	2.104(3)	P2: 4.722
−O3	2.1365(18)	−O3	2.117(3)	O1: 0.354
−O4	2.1372(19)	−O4	2.115(3)	O2: 0.329
−O2$_{H2O}$	2.145(2)	−O2$_{H2O}$	2.091(4)	O3: 1.908
Fe2−O5	2.0749(19)	Co2−O5	2.048(3)	O4: 1.899
−O1$_{H2O}$	2.118(2)	−O1$_{H2O}$	2.062(4)	O5: 1.583
−O4	2.1516(19)	−O4	2.126(3)	O6: 1.867
−O3	2.167(2)	−O3	2.147(3)	O7: 1.800
−O6	2.1812(18)	−O6	2.139(3)	O8: 1.084
−O7	2.1925(19)	−O7	2.168(3)	O9: 1.061
P1−O3	1.5183(19)	P1−O3	1.521(3)	**CoGePO**
−O4	1.5246(19)	−O4	1.518(3)	Ge1: 4.288
−O10	1.5375(19)	−O10	1.542(3)	Co1: 1.985
−O9$_H$	1.582(2)	−O9$_H$	1.577(3)	Co2: 1.927
P2−O6	1.5330(19)	P2−O6	1.531(3)	P1: 4.771
−O5	1.541(2)	−O5	1.536(3)	P2: 4.756
−O7	1.5480(19)	−O7	1.541(3)	O1: 0.368
−O11	1.5485(19)	−O11	1.552(3)	O2: 0.340
O1−H1	0.806 (19)	O1−H1	0.81(2)	O3: 1.861
O1−H2	0.80(2)	O1−H2	0.82(2)	O4: 1.890
O2−H3	0.804(19)	O2−H3	0.83(2)	O5: 1.584
O2−H4	0.832(19)	O2−H4	0.83(2)	O6: 1.783
O8−H5	0.86	O8−H5	0.82	O7: 1.809
O9−H6	0.81(2)	O9−H6	0.81(2)	O8: 1.080
				O9: 1.076

pentamers, resulting in a 3-D framework structure. The $[GeP_4O_{14}(OH)_4]^{8-}$ pentamer is made of a central $GeO_4(OH)_2$ octahedron linked by its four equatorial vertices to two PO_4 tetrahedra and two $PO_3(OH)$ groups via common O-corners (Figure 2, middle). The remaining two trans-hydroxyl apexes of the $GeO_4(OH)_2$ octahedron together with the O-corners of phosphate groups in the $[GeP_4O_{14}(OH)_4]^{8-}$ pentamer are further linked to four zigzag $M^{II}O_6$-octahedral chains running along $[10\bar{1}]$ which consist of alternate $M^{II}O_4(OH)(H_2O)$ and $M^{II}O_5(H_2O)$ octahedra by sharing either skew- or trans-edges (Figure 2, left).

In the following, **FeGePO** is chosen as a representative example for discussion because the two compounds are isostructural. The asymmetric unit of **FeGePO** contains one Ge atom with octahedral coordination, two crystallographically distinct P atoms both with tetrahedral coordination, and two distinct Fe atoms in octahedral coordination (see Figure 3a). Fe1 is surrounded by four O atoms, one OH group, and a water molecule with an average bond length of Fe1−O$_{av}$ = 2.132 Å. Fe2 coordinates to five O atoms and one water molecule (Fe2−O$_{av}$ = 2.148 Å). The Fe−O distances of both iron sites are close to those expected for Fe(II) oxides. Ge1 is located at the inversion center and adopts slightly distorted octahedral coordination with its four O-atoms in the basal plane linked to four PO_4 tetrahedra and two OH groups to FeO_6 octahedra at the trans-position. The Ge−O distances are in the range of 1.8592(19)−1.9042(19) Å with an average bond length of 1.880 Å, which is comparable with germanium in octahedral coordination observed in germanates[6−10,12] and transition metal germanophosphates.[18−20] Both P1 and P2 atoms occupy the general position. P1 has a regular tetrahedral coordination of neighboring oxygen (P1−O$_{av}$ = 1.541 Å). P2 has a slightly distorted tetrahedral coordination with a terminal OH-group (P2−O$_{av}$ = 1.543 Å). Bond valence calculations[25] indicate that the Ge atom is in the +4 state, P atoms are in the +5 state, while Fe atoms at both sites are in the +2 state which is further confirmed by the magnetic measurements and Mössbauer study discussed below. The detailed values of bond valence sums are given in Table 2. For the cobalt compound, the coordination environments of all atoms are quite similar to the isotypic Fe-compound except for the slightly shorter bond lengths, which is consistent with the smaller ionic radius of Co.

The FeO_6 octahedra adopt an edge-sharing arrangement. The $Fe2O_5(OH_2)$-octahedra share their trans-edges with two $Fe1O_4(OH)(OH_2)$-octahedra, and Fe1-octahedra in turn share skew-edges with two Fe2-octahedra, resulting in a zigzag chain with a "trans skew trans skew" manner of FeO_6 octahedra running along $[10\bar{1}]$ (Figure 2, left). This type of zigzag iron-octahedral chain has been reported in several ferrous diphosphates, such as $SrFe_3(P_2O_7)_2$[26] and $(NH_4)_2[Fe_3(H_2O)_2(P_2O_7)_2]$.[27] In the ferrous diphosphates, the zigzag chains are separated by pyrophosphate units. While in the title compound, the separation is increased further by the more complex germanophosphate pentamers.

The germanophosphate anionic partial structure can be described as $[GeP_4O_{14}(OH)_4]^{8-}$ pentamer, which is built from a central $GeO_4(OH)_2$ octahedron linked by its four equatorial vertices to two P1-tetrahedra and two P2-tetrahedra via common O-corners (see Figure 2, middle). The isolated $[GeP_4O_{14}(OH)_4]^{8-}$ pentamer is the first time to be observed in the germanophosphate system. The pentamers, furthermore, act as ligands to link adjacent four FeO_6-based zigzag chains by sharing the O-atoms of PO_4 tetrahedra and OH-groups of GeO_6 octahedra (Figure 3b), resulting in a 3-D framework structure with eight-membered ring channels parallel to [100] (see Figure 4a). Consequently, it results in four 3-coordinated oxygen atoms, four 2-coordinated oxygen atoms, and three terminal oxygen

dx.doi.org/10.1021/ic202773p | Inorg. Chem. 2012, 51, 3316−3323

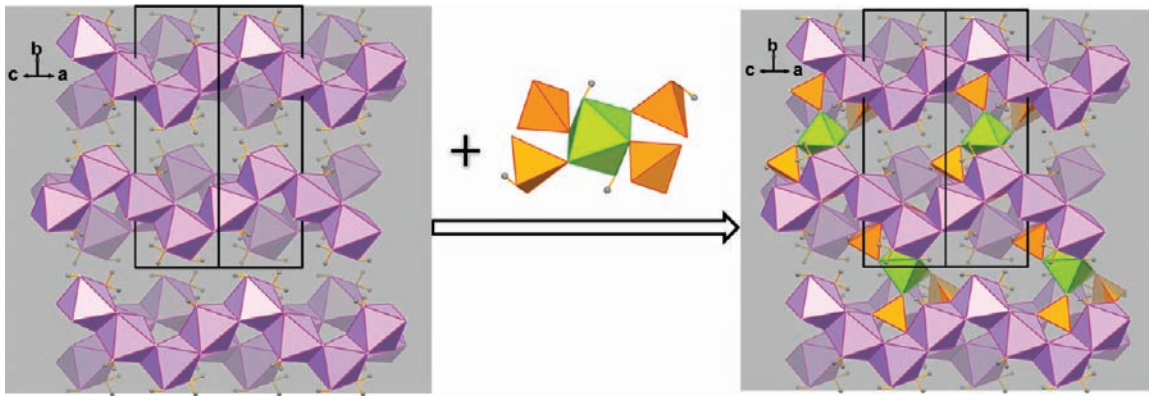

Figure 2. The one-dimensional zigzag $M^{II}O_6$-octahedral chains of $M^{II}_4(H_2O)_4[Ge(OH)_2(HPO_4)_2(PO_4)_2]$ (M^{II} = Fe, Co), running along [10$\bar{1}$], are built from $M^{II}O_5(H_2O)$ and $M^{II}O_4(OH)(H_2O)$ octahedra by sharing common edges in an alternating fashion (left), which are interconnected by $GeP_4O_{14}(OH)_4^{8-}$ pentamers (middle) along [010] and [101], resulting in three-dimensional neutral networks (right). Purple octahedra, $M^{II}O_6$; green octahedra, GeO_6; orange tetrahedra, PO_4; medium gray spheres, H atoms.

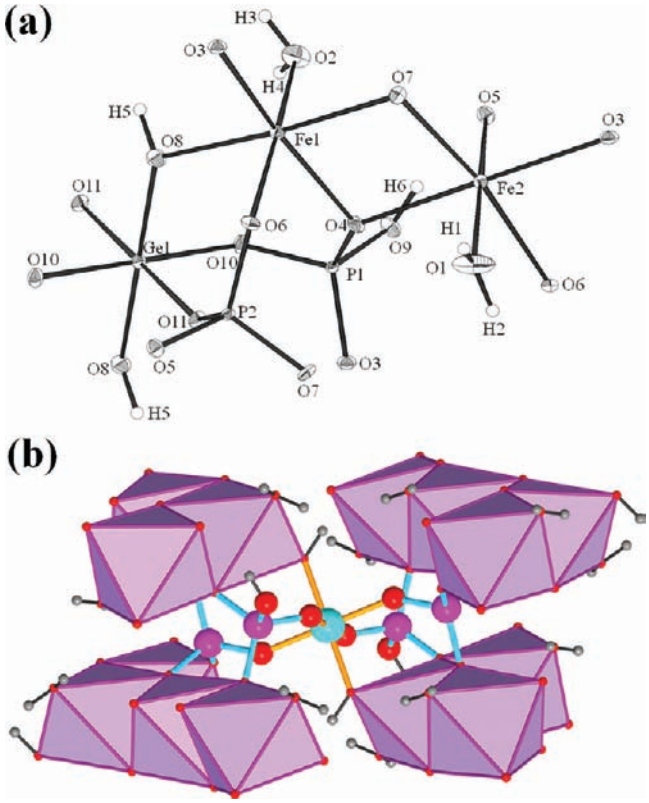

Figure 3. (a) Coordination environments of Fe, Ge, and P atoms with the ellipsoid drawn at the 50% probability. (b) The $GeP_4O_{14}(OH)_4^{8-}$ pentamer links four $M^{II}O_6$-octahedral single chains via O/OH-corners. Purple octahedron, $M^{II}O_6$; cyan sphere, Ge atom; purple sphere, P atom; red sphere, O atom; medium gray sphere, H atom.

atoms. The O3, O4, O6, and O7 atoms, besides bonding to P, also bond to two adjacent iron atoms and hence are 3-coordinate. Whereas, O5, O8, O10, and O11 atoms are 2-coordinate, O5 forming a P−O−Fe bridge, O8 as an OH group forming a Fe−O−Ge bridge, the latter two forming a P−O−Ge bridge. The O9 appeared to be an OH group that is coordinated to P1 solely and points into the eight-membered ring channels. The O1 and O2 atoms in the coordination sphere of Fe1 and Fe2 also point to eight-membered ring channels. Both are assigned as coordinated water molecules that are confirmed by the location of hydrogen atoms in the difference Fourier map together with the IR spectrum and bond valence calculation (−0.354 and −0.329 for O1 and O2, respectively).

The crystal structures of title compounds, similar to two known transition metal germanophosphates, $[Cu(H_2O)_2(OH)]_2Ge(PO_4)_2$[19] and $CdGe(OH)_3PO_4$,[20] possess M^{II}−O−M^{II} octahedral single chains. However, the conformation of transition metal octahedral chains and the connection between germanates and phosphates are quite different (see Figure 4). For the linkage of transition metal chains, octahedra share both trans-edges and skew-edges in the title compounds, while they only share trans-apical corners in the Cu-compound and trans-edges in the Cd-compound. For the germanophosphate anionic structures, $[GeP_4O_{14}(OH)_4]^{8-}$ pentamers in the title compound are isolated, while single chains built from the condensation of $[GeP_4O_{14}(OH)_4]^{8-}$ pentamers by sharing two common phosphate groups are presented in the Cu-compound. Furthermore, in the Cd-compound, germanate octahedra share trans O-corners to form a linear chain that is loop-branched by PO_4 tetrahedra alternately through corner-sharing. The large variety connections of germanate and phosphate groups shown here, from oligomer to single chain and even to framework, imply a very rich structural chemistry for germanophosphates. Additionally, the title compounds display one or two antiferromagnetic ordering transitions at low temperature. When considering the diverse connections of transition metals and its magnetic properties, together with the rich structure chemistry of germanophosphate anionic structure, the system of transition metal−phosphate−germanate will open a new field not only for chemists but also for physicists.

3.2. Infrared spectroscopy. The FTIR spectra of **CoGePO** and **FeGePO** show similar absorption bands (see Figure 5). The peaks at 3420/3428 (shoulder, medium) cm^{-1} can be attributed to the asymmetric O−H stretching, while the peaks at 1635 cm^{-1} (sharp, strong) and 3591/3596 cm^{-1} (sharp, weak) are assigned to the H−O−H bending mode. The peaks at 1290/1296 cm^{-1}(sharp, strong) are assigned to the Ge−OH vibrations as observed in $CdGe(OH)_3PO_4$.[20] These absorption bands verify the presence of the OH groups and water molecules in the structure

3.3. Thermal Analysis. TGA results, investigated under static air atmosphere up to 800 °C, are shown in Figure 6a. A single step weight loss of 13.29% was observed at the temperature range of 300−600 °C in the TG curve of **CoGePO**, which can be assigned to the removal of 6 × H_2O per formula unit (calcd, 13.56%). However, a two-step weight loss and a less value were

dx.doi.org/10.1021/ic202773p | Inorg. Chem. 2012, 51, 3316−3323

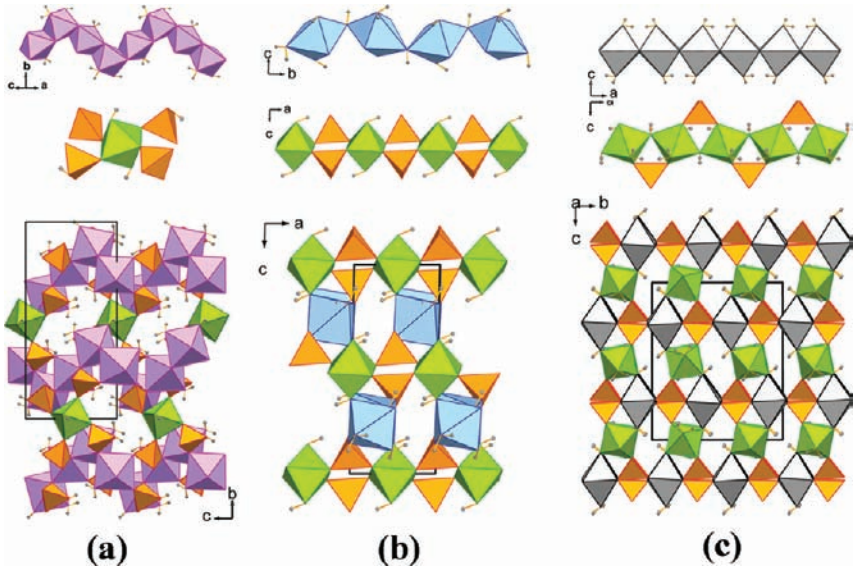

Figure 4. Three structural motifs of transition metal germanophosphates: (a) $M^{II}_4(H_2O)_4[Ge(OH)_2(HPO_4)_2(PO_4)_2]$ (M^{II} = Fe, Co) (this work), (b) $[Cu(H_2O)_2(OH)]_2Ge(PO_4)_2$,[19] and (c) $CdGe(OH)_3(PO_4)$,[20] built from M^{II}–O–M^{II} octahedral chains interconnected by different germanophosphate anionic partial structures. Purple octahedra, $M^{II}O_6$; blue octahedra, CuO_6; gray octahedra, CdO_6; green octahedra, GeO_6; orange tetrahedra, PO_4; medium gray spheres, H atoms.

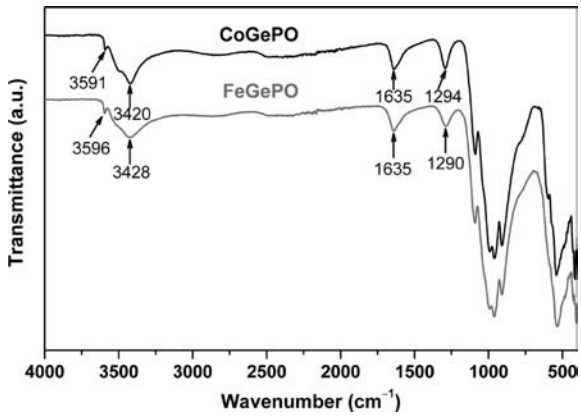

Figure 5. Infrared spectra (IR) of **FeGePO** (lower) and **CoGePO** (upper).

found for the isotypic iron compound (**FeGePO**) in the temperature range of 250–700 °C. The observed value of 9.73% is not consistent with the expected one (calcd, 13.78%; removal of 6 × H_2O per formula unit) as that of the cobalt-compound. In order to understand why **FeGePO** exhibits two weight loss steps and has less weight loss than those of **CoGePO**, the residuals after TG analyses were checked by powder X-ray diffraction. The mixture of $Fe^{III}PO_4$[28] and GeO_2[29] were identified for the TG residual of **FeGePO**, while the mixture of $Co_2P_2O_7$[30] and GeO_2[29] for **CoGePO**. Thus, the decomposition reactions of the title compounds can be proposed as follows:

$$Co^{II}_4(H_2O)_4[Ge(OH)_2(HPO_4)_2(PO_4)_2] \rightarrow 2Co^{II}_2P_2O_7 + GeO_2 + 6H_2O$$

$$Fe^{II}_4(H_2O)_4[Ge(OH)_2(HPO_4)_2(PO_4)_2] + O_2 \rightarrow 4Fe^{III}PO_4 + GeO_2 + 6H_2O$$

According to the reaction equations, the less weight loss of the iron compound is mostly due to the oxidation of Fe^{2+} to

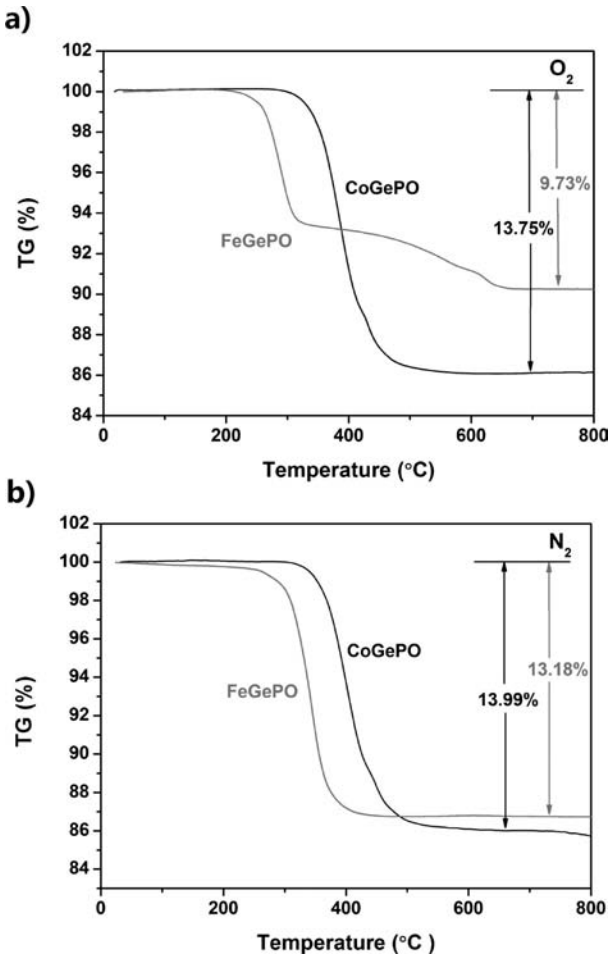

Figure 6. Thermogravimetric curves of **FeGePO** and **CoGePO** conducted under (a) static air and (b) N_2 atmosphere.

Fe^{3+}, which gains one O_2 molecule from air (~4.08% per formula unit of **FeGePO**). In order to verify this assumption,

dx.doi.org/10.1021/ic202773p | Inorg. Chem. 2012, 51, 3316–3323

we further performed TGA under N_2 atmosphere. The TG curves (Figure 6b) show single step weight loss (13.18% for **FeGePO** and 13.99% for **GoGePO**) for both compounds. Such a result is consistent very well with our above hypothesis. For **FeGePO**, the additional second weight loss step determined in air is mainly caused by the oxidization of Fe^{2+} to Fe^{3+} as well. It is noteworthy that the less weight loss, in turn, confirms that iron is present as Fe^{2+} in the compound but not Fe^{3+}, which is demonstrated in the next sections.

3.4. Mössbauer Study. The powder Mössbauer resonance spectra were measured at room temperature in transmission geometry by use of a constant acceleration spectrometer and a ^{57}Co source diffused into a rhodium matrix. The velocity scale was calibrated with α-Fe foil at room temperature. The spectra were fitted using MossWinn 4.0.[31] The isomer shift values are given with respect to α-Fe at 293 K. Figure 7 shows the

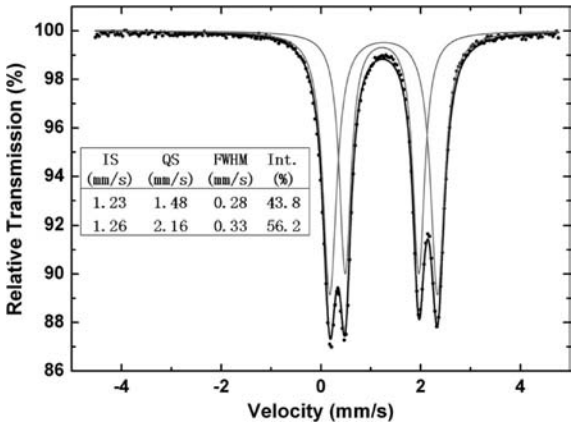

Figure 7. ^{57}Fe Mössbauer spectrum for **FeGePO** recorded at room temperature (with a ^{57}Co/Rh radiation source).

Mössbauer spectrum of a powder sample of **FeGePO** recorded at room temperature. The spectrum contains two quadrupole doublets with large isomer shifts (IS, 1.22 and 1.26 mm s^{-1}) and large quadrupole splitting (QS, 1.48 and 2.16 mm s^{-1}). Such isomer shifts and quadrupole splits are characteristic of divalent iron in octahedral coordination.[32] The larger QS for the second site may indicate more distorted octahedral coordination. The two quadrupole doublets with intensities of 43.8% and 56.2%, respectively, indicate that there are two sites for divalent iron in almost equal proportion in the structure of **FeGePO**.

3.5. Magnetic Properties. The magnetic properties of the title compounds have been investigated in a SQUID magnetometer. Figure 8a shows the temperature dependence of the magnetic susceptibility for **FeGePO**. For temperatures above 100 K, a Curie−Weiss law is observed with a Weiss temperature θ = +27.8 K and effective magnetic moment μ_{eff}/Fe-atom = 5.67μ_B. At lower temperatures, the antiferromagnetic long-range order of the Fe-moments is found. The Néel temperature T_N = 19.3 K is determined from a sharp maximum in the derivative of the product χT with temperature (Figure 8a, inset). A rounded maximum in $\chi(T)$ at 23 K reveals that the dominant exchange interactions are low-dimensional and probably within the one-dimensional octahedral chain structures. From the effective magnetic moment, the chemical valence of iron cannot be determined unambiguously, since 5.7μ_B is occasionally observed for both Fe^{2+} and Fe^{3+} in octahedral coordination. In order to study the magnetically

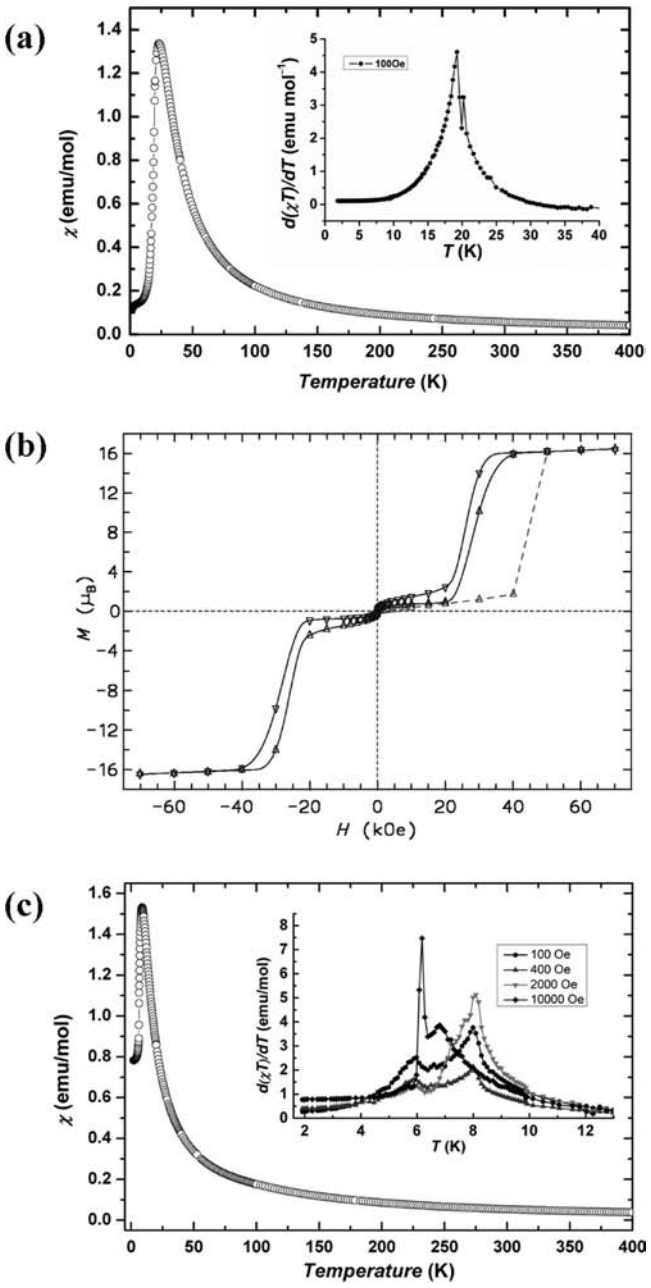

Figure 8. (a) Temperature dependence of the molar magnetic susceptibility $\chi(T)$ of **FeGePO** for an external field of 10 kOe. The inset shows the derivative $d(\chi T)/dT$ for H_{ext} = 100 Oe. (b) Isothermal magnetization curve at 1.8 K for **FeGePO** with magnetic fields up to 70 kOe. The triangle directions (up or down) indicate the field sweep direction. The initial curve is marked by a dashed line, the other segments by a full line (as guides to the eye). (c) Temperature dependence of the molar magnetic susceptibility $\chi(T)$ for **CoGePO** in H_{ext} = 10 kOe. The inset shows the derivative $d(\chi T)/dT$ in different external fields: 100 Oe (black, circle), 400 Oe (medium gray, triangle), 2 kOe (light gray, down triangle), 10 kOe (black, diamond).

ordered state of **FeGePO**, isothermal magnetization curves were measured below T_N. The curve at 1.8 K (Figure 8b) is strongly nonlinear and shows hysteresis. A weak moment is induced already at very low fields. This basically still antiferromagnetic state starts to break up at fields around 28 kOe. A metamagnetic transition takes place above which the magnetic moment increases only very slowly. The saturation magnetization of μ_{Fe} = 4.0μ_B per Fe-atom fits well to the

dx.doi.org/10.1021/ic202773p | Inorg. Chem. 2012, 51, 3316−3323

theoretical saturation moment expected for a high-spin Fe^{2+} ($3d^6$) species ($\mu_{Fe} = 2S\mu_B = 4\mu_B$) for octahedral coordination. This is also a clear confirmation for the presence of Fe^{2+} species.

The magnetic susceptibility $\chi(T)$ of **CoGePO** is clearly different from that of the isomorphic iron compound (see Figure 8c). The data reveal the presence of two magnetic ordering transitions at $T_{N1} \approx 8$ K and $T_{N2} \approx 6$ K. These transitions are better seen as peaks in the derivative of χT with respect to T (inset of Figure 8c). The transition at T_{N1} can be attributed to the transition from the paramagnetic to an antiferromagnetic ordered state, in agreement with the decrease of T_{N1} with increasing field. In contrast, the transition at T_{N2} does not move with increasing the field to 10 kOe, however it gets more pronounced. It can be attributed to a spin-reordering transition. As in the Fe-compound there is a metamagnetic transition (a spin-flop) at ≈22 kOe seen in the magnetization curve at 1.8 K (not shown). No weak ferromagnetism is observed in both magnetic phases. In the paramagnetic range, $\chi(T)$ shows ferromagnetic correlations increasing toward lower T (no reasonable Curie−Weiss fit is possible). While we expect also in **CoGePO** low-dimensional magnetic correlations within the octahedral chains, no maximum of $\chi(T)$ is seen above the long-range magnetic ordering temperature T_{N1}.

4. CONCLUSION

In this paper, we have demonstrated the great potential of the transition metal germanophosphate system for the new framework combined with interesting magnetic properties. Here the syntheses, X-ray structure analyses, Mössbauer spectroscopy, and magnetic measurements of two isostructural transition metal germanophosphates have been carried out. Their crystal structure is built from zigzag chains of $M^{II}O_6$ octahedra by sharing either trans or skew edges, interconnected by $[GeP_4O_{14}(OH)_4]^{8-}$ pentamers, resulting in a neutral 3-D framework. The isothermal magnetization and Mössbauer study confirm the presence of Fe^{2+} species in the iron compound. The less weight loss in air than in N_2 atmospheres during the thermal analysis further confirm the presence of Fe^{2+} in the iron compound. Note that there are two antiferromagnetic ordering transitions (at around 8 and 6 K) for **CoGePO**, whereas one is seen (at 19 K) for **FeGePO**. A rounded maximum observed in $\chi(T)$ of **FeGePO** indicates low-dimensional magnetic correlations within the octahedral chains structures. The rich structure chemistry and magnetic properties of the known transition metal germanophosphates suggest that investigation of the field of transition metal germanophosphate should be encouraged.

■ ASSOCIATED CONTENT

Ⓢ Supporting Information

Figures of experimental and simulated powder X-ray diffraction patterns and crystallographic information files in CIF format. This material is available free of charge via the Internet at http://pubs.acs.org.

■ AUTHOR INFORMATION

Corresponding Author

*E-mail: yaxihuang@xmu.edu.cn. Phone: +86-13950175872. Fax: +86-592-2183937.

Notes

The authors declare no competing financial interest.

■ ACKNOWLEDGMENTS

This work was supported by Scientific Research Foundation for the Returned Overseas Chinese Scholars of State Education Ministry, the National Natural Science Foundation of China (Grant No. 40972035), the Natural Science Foundation of Fujian Province of China (Grant No. 2010J01308), and Scientific and Technological Innovation Platform of Fujian Province of China (Grant No. 2009J1009). We are grateful to Dr. Gudrun Auffermann and Anja Völzke for elemental analyses as well as Stefan Hoffmann and Susann Scharsach for thermal analyses in MPI CPfS. We also thank Yan Zhou for the IR measurements.

■ REFERENCES

(1) Zubieta, J. *Comments Inorg. Chem.* **1994**, *16*, 153−183.
(2) Brock, S. L.; Duan, N. G.; Tian, Z. R.; Giraldo, O.; Zhou, H.; Suib, S. L. *Chem. Mater.* **1998**, *10*, 2619−2628.
(3) Padhi, A. K.; Nanjundaswamy, K. S.; Goodenough, J. B. *J. Electrochem. Soc.* **1997**, *144*, 1188−1194.
(4) Whittingham, M. S.; Song, Y. N.; Lutta, S.; Zavalij, P. Y.; Chernova, N. A. *J. Mater. Chem.* **2005**, *15*, 3362−3379.
(5) Centi, G.; Trifiro, F.; Ebner, J. R.; Franchetti, V. M. *Chem. Rev.* **1988**, *88*, 55−80.
(6) Bu, X. H.; Feng, P. Y.; Stucky, G. D. *J. Am. Chem. Soc.* **1998**, *120*, 11204−11205.
(7) Li, H.; Eddaoudi, M.; Richardson, D.; Yaghi, O. *J. Am. Chem. Soc.* **1998**, *120*, 8567−8568.
(8) Bu, X. H.; Feng, P. Y.; Stucky, G. D. *Chem. Mater.* **2000**, *12*, 1811−1813.
(9) Zou, X. D.; Conradsson, T.; Klingstedt, M.; Dadachov, M. S.; O'Keeffe, M. *Nature* **2005**, *437*, 716−719.
(10) Pan, Q. H.; Li, J. Y.; Christensen, K. E.; Bonneau, C.; Ren, X. Y.; Shi, L.; Sun, J. L.; Zou, X. D.; Li, G. H.; Yu, J. H.; Xu, R. R. *Angew. Chem., Int. Ed.* **2008**, *47*, 7868−7871.
(11) Lin, C.-H.; Lii, K.-H. *Angew. Chem., Int. Ed.* **2008**, *47*, 8711−8713.
(12) Lin, Z.-E.; Yang, G.-Y. *Eur. J. Inorg. Chem.* **2010**, 2895−2902.
(13) Alami, M.; Brochu, R.; Soubeyroux, J. L.; Gravereau, P.; Flem, G. L.; Hagenmuller, P. *J. Solid State Chem.* **1991**, *90*, 185−193.
(14) Zhao, D.; Xie, Z.; Hu, J.-M.; Zhang, H.; Zhang, W.-L.; Yang, S.-L.; Cheng, W.-D. *J. Mol. Struct.* **2009**, *922*, 127−134.
(15) Brochu, R.; Loueer, M.; Alami, M.; Alquraoui, M.; Loueer, D. *Mater. Res. Bull.* **1997**, *32*, 113−122.
(16) Winand, J.-M.; Rulmont, A.; Tarte, P. *J. Solid State Chem.* **1993**, *107*, 356−361.
(17) Engel, G.; Fischer, U. *Z. Kristallogr.* **1985**, *173*, 101−112.
(18) Li, J. M.; Ke, Y. X.; Zhang, Y. G.; He, G. F.; Jiang, Z.; Nishiura, M.; Imamoto, T. *J. Am. Chem. Soc.* **2000**, *122*, 6110−6111.
(19) Liu, Y.; Yang, X. L.; Zhang, J.; Li, Y. Z.; Song, Y.; Du, H. B.; You, X. Z. *Chem. Commun.* **2008**, 3145−3147.
(20) Liu, Y.; Yang, X. L.; Wang, G. L.; Zhang, J.; Li, Y. Z.; Du, H. B.; You, X. Z. *J. Solid State Chem.* **2008**, *181*, 2542−2546.
(21) Guse, W.; Klaska, K. H.; Saalfeld, H.; Adiwidjaja, G. *Neues Jahrb. Mineral. Monat* **1985**, *10*, 433−438.
(22) Mayer, H.; Völlenkle, H. *Z. Kristallogr.* **1972**, *136*, 387−401.
(23) Sheldrick, G. M. *Acta Crystallogr., Sect. A: Found. Crystallogr.* **2008**, *64*, 112−122.
(24) Farrugia, L. J. *J. Appl. Crystallogr.* **1999**, *32*, 837−838.
(25) Brese, N. E.; M., O. K. *Acta Crystallogr., Sect. B: Struct. Sci.* **1991**, *47*, 192−197.
(26) Lii, K. H.; Shih, P. F.; Chen, T. M. *Inorg. Chem.* **1993**, *32*, 4373−4377.
(27) Liu, B.; Zhang, X.; Wen, L.; Sun, W.; Huang, Y.-X. *Acta Crystallogr., Sect. E: Struct. Rep. Online* **2011**, *68*, i5−i6.
(28) Labeguerie, P.; Harb, M.; Baraille, I.; Rerat, M. *Phys. Rev. B* **2010**, *81*, 045107.

(29) Haines, J.; Cambon, O.; Philippot, E.; Chapon, L.; Hull, S. *J. Solid State Chem.* **2002**, *166*, 434−441.
(30) El Bali, B.; Bolte, M. *Acta Crystallogr., Sect. E: Struct. Rep. Online* **2002**, *58*, i32−i33.
(31) Klenczar, Z.; Kuzmann, E.; Vertes, A. *J. Rad. Nucl. Chem.* **1996**, *210*, 105−118.
(32) Etourneau, J.; Portier, J.; Menil, F. *J. Alloys Compd.* **1992**, *188*, 1−7.